Medical Image Analysis 16 (2012) 786–795

Contents lists available at SciVerse ScienceDirect

Medical Image Analysis

journal homepage: www.elsevier.com/locate/media

Mass preserving image registration for lung CT

Vladlena Gorbunova [a,*], Jon Sporring [a], Pechin Lo [a], Martine Loeve [b], Harm A. Tiddens [b], Mads Nielsen [a,c], Asger Dirksen [d], Marleen de Bruijne [a,e]

[a] Image Group, Department of Computer Science, University of Copenhagen, Denmark
[b] Department of Pediatric Pulmonology and Allergology and Radiology, Erasmus Medical Center, Rotterdam, The Netherlands
[c] Nordic Bioscience A/S, Denmark
[d] Department of Respiratory Medicine, Gentofte University Hospital, Denmark
[e] Biomedical Imaging Group Rotterdam, Department of Radiology and Medical Informatics, Erasmus Medical Center, Rotterdam, The Netherlands

ARTICLE INFO

Article history:
Received 27 August 2010
Received in revised form 6 November 2011
Accepted 7 November 2011
Available online 14 January 2012

Keywords:
Image registration
B-Splines
Mass preservation
Lung CT

ABSTRACT

This paper presents a mass preserving image registration algorithm for lung CT images. To account for the local change in lung tissue intensity during the breathing cycle, a tissue appearance model based on the principle of preservation of total lung mass is proposed. This model is incorporated into a standard image registration framework with a composition of a global affine and several free-form B-Spline transformations with increasing grid resolution. The proposed mass preserving registration method is compared to registration using the sum of squared intensity differences as a similarity function on four groups of data: 44 pairs of longitudinal inspiratory chest CT scans with small difference in lung volume; 44 pairs of longitudinal inspiratory chest CT scans with large difference in lung volume; 16 pairs of expiratory and inspiratory CT scans; and 5 pairs of images extracted at end exhale and end inhale phases of 4D-CT images. Registration errors, measured as the average distance between vessel tree centerlines in the matched images, are significantly lower for the proposed mass preserving image registration method in the second, third and fourth group, while there is no statistically significant difference between the two methods in the first group. Target registration error, assessed via a set of manually annotated landmarks in the last group, was significantly smaller for the proposed registration method.

1. Introduction

Registration of lung CT images is increasingly used in various clinical applications. Three main applications may be distinguished as follows (Sluimer et al., 2006): atlas registration based segmentation of the lungs and structures within the lungs; registration of longitudinal CT image series to monitor disease progression; registration of successive frames in dynamic CT sequences to estimate local ventilation and perfusion.

Examples of the first application can be found in (Sluimer et al., 2005; Zhang et al., 2006). Sluimer et al. (2005) proposed to segment lungs containing dense pathologies by non rigidly registering a set of segmented example images to the image to segment and propagating their labels, while Zhang et al. (2006) used atlas registration to initialize fissure detection for lung lobe segmentation. Registration of scans of the same patient taken at different points in time is applied for instance in the monitoring of lung nodules, both to robustly match nodules in sequential CT scans (Hong et al., 2008; Zheng et al., 2007) and to visualize nodule changes over time (Staring et al., 2007). Recently, registration was also applied to estimate local emphysema progression from longitudinal image data (Gorbunova et al., 2008; Staring et al., 2009). Registration of successive time frames of 4D-CT lung images is used for motion estimation in lung cancer radiotherapy planning (Boldea et al., 2008; Guerrero et al., 2005; Li et al., 2008) and for estimation of regional lung ventilation (Reinhardt et al., 2008; Kabus et al., 2008; Ue et al., 2007; Guerrero et al., 2006; Ding et al., 2010). Expiratory lung CT scans were registered to inspiratory scans to help detect air trapping and facilitate classification of pulmonary diseases (Murphy et al., 2009).

A crucial factor in image registration is the choice of a similarity measure describing the (dis) similarity between the fixed and the deformed images. Commonly used image similarity functions are the sum of squared differences (SSDs), mutual information (MI) and normalized cross correlation (NCC) (Hill et al., 2001). For intra-subject registration of lung CT images, which is the case we consider in this paper, SSD is probably the most commonly used similarity measure (Wu et al., 2008; Zheng et al., 2007; Reinhardt et al., 2008; Christensen et al., 2007; Pevsner et al., 2006; Sarrut et al., 2006). Sum of squared differences is optimal when

* Corresponding author. Mobile: +49 157 869 38 047.
E-mail addresses: vladlena@diku.dk (V. Gorbunova), marleen@diku.dk (M. de Bruijne).

1361-8415/$ - see front matter © 2012 Elsevier B.V. All rights reserved.
doi:10.1016/j.media.2011.11.001

corresponding anatomical points are represented by the same intensity in the images, with additional Gaussian noise. In the case of CT, where the Hounsfield unit (HU) represents the density of tissue which is often expected to remain constant, this is usually a valid assumption. However, in the lungs the density of tissue depends on the amount of air present and can therefore vary drastically, both spatially and in time Shaker et al. (2004) and Sarrut et al. (2006). The basic assumption of the SSD similarity function thus does not hold for lung tissue and, as a possible solution, we propose to model appearance of lung tissue in CT scan with respect to the regional ventilation using a simple law of mass preservation.

In this mass preserving model, the density of the lung tissue is inversely proportional to the local volume. Therefore change in local volume can be computed from the change in the density. Simon (2000) applied such a model to estimate regional ventilation from image intensity in 4D-CT lung scans. Vice versa, the change in density of the lung tissue can be computed from the change in the local volume. Under applied local deformations, the absolute value of the Jacobian determinant defines the factor by which the deformation expands/contracts the volume. Therefore the density of the lung tissue can be computed from the Jacobian determinant of the deformations. Recently, Reinhardt et al. (2008) showed strong correlation between regional ventilation obtained from Xe-CT imaging and the ventilation estimated using an image registration procedure. In the latter case, regional ventilation was defined as the Jacobian determinant of the obtained transformation between two images.

In this paper, we propose to model the lung tissue density using the determinant of the Jacobian of the transformation function. We modified the sum of squared differences similarity function to enable mass preservation and simulate the appearance of the lung tissue under the given deformations. Early version of this work appeared in (Gorbunova et al., 2008; Gorbunova et al., 2009), where the mass preserving algorithm was applied to the longitudinal breath-hold lung CT scans (Gorbunova et al., 2008) and to the pairs of maximum inspiration and maximum expiration CT scans taken on the same day (Gorbunova et al., 2009). Since then a similar idea has been used by Yin et al. (2009a) and Yin et al. (2009b), where the mass preserving image registration was applied to breath-hold lung CT images acquired at the maximum inspiration and maximum expiration in the same scanning session.

Several recent studies have successfully incorporated mass preserving assumption in registration process. Sarrut et al. (2006) proposed to modify lung density in a 4D-CT image prior to registration. Zhu et al. (2007) proposed a new registration method which establishes the optimal mass transportation between the images while the image intensities remain constant. Castillo et al. (2009a) proposed to incorporate the mass preserving intensity modification model into the optical-flow registration and applied it to the 4D-CT images.

In this paper, we present the registration framework in more detail, investigate the assumption of mass preservation, and present a quantitative evaluation of registration accuracy of the proposed mass preserving image registration method compared to an image registration method with the SSD similarity function on a large number of CT scans of varying quality, ranging from small to large differences in inspiration level.

2. Mass preserving image registration

This section briefly presents a general deformable image registration framework based on B-Splines which is used in many medical imaging tasks (Rueckert et al., 1999; Mattes et al., 2003), and explains how the proposed mass preserving methodology can be incorporated in this framework.

2.1. Image registration outline

Consider a pair of images I_f and I_m, referred to as fixed image and moving image respectively. The task of registration is to find for every point in the fixed image domain Ω_f the corresponding point in the moving image domain Ω_m. The obtained point correspondences define a general transformation function $T{:}\Omega_f \rightarrow \Omega_m$. Validity of the transformation can be assessed by comparing the deformed moving image and the fixed image using a dissimilarity function $C(I_f, I_m \circ T)$. An optimal transformation should minimize the dissimilarity between the deformed and fixed image, therefore the registration process can be formulated as a minimization problem, as follows,

$$\underset{T}{argmin}(C(I_f, I_m \circ T)).$$

2.2. Preprocessing

To avoid errors near the lung surface which are caused by the sliding motion of lungs along the chest wall during breathing, only the image information inside the lungs is used for registration. Segmentations of the lung fields are obtained using region growing and morphological smoothing (Lo et al., 2010) and the background region is set to a constant value of 0 HU. Finally, the image intensities are shifted with a value 1000 HU so that the new intensities approximate the real densities of the tissues.

2.3. Transformation

We follow a common approach and use a multi-resolution image registration strategy. First, the images are registered affinely. To provide an accurate initialization of the affine transformation, the trachea and main bronchi are first extracted using a modified fast marching algorithm (Lo et al., 2010). The center of the affine transformation is then set at the carina point in the fixed image and the initial translation is set to the difference between the carina points in moving and fixed images. Secondly, a series of B-Spline transformations, with corresponding Gaussian smoothing at the coarser levels, is applied to the pre-aligned, regridded images. The final transformation is thus a composition of a global affine transformation T_A and N levels of B-Spline transformations $T^i_{B-Spline}$ with decreasing grid size:

$$T_{final}(\mathbf{x}) = T^N_{B-Spline} \circ \ldots \circ T^1_{B-Spline} \circ T_A(\mathbf{x}), \quad (1)$$

where $\mathbf{x} = (x_1, x_2, x_3)$ is a point in the fixed image domain Ω_f.

In this work, we have used small step size along the gradient and multi-level B-Spline grid to ensure that the transformation is invertible (Rueckert et al., 2006).

2.4. Mass preserving similarity function

We use the sum of squared differences similarity function as the basis for the mass preserving similarity measure,

$$C(I_f, I_m \circ T) = \frac{1}{|\Omega_f|} \|I_f(\mathbf{x}) - I_m(T(\mathbf{x}))\|^2_{L_2}, \quad (2)$$

where $\mathbf{x}$ is a point in the region Ω_f occupied by the fixed image I_f, and $\mathbf{y} = T(\mathbf{x})$ is the corresponding point in the region Ω_m occupied by the moving image I_m.

The sum of squared differences is an optimal similarity measure if image intensities are identical or differ with Gaussian noise. This assumption does not hold in case of lung CT images, where during inhalation both blood and air enter the lungs. We used a hypothesis that most of the incoming blood stays in the larger vessels, and only air is inhaled into the alveoli. Therefore we can assume that

mass of parenchyma remains constant and the density of lung tissue is inversely proportional to the amount of air. Under the applied local deformations, the induced change in local volume is defined by the determinant of Jacobain of the associated transformation function.

Using the mass preserving assumption, the intensity of the moving image I_m in a point $\mathbf{y} \in \Omega_M$ is inversely proportional to the change in local volume $det(J_{T^{-1}})$ in the point $\mathbf{y}$. The modeled intensity can be written as $\widehat{I}_m(\mathbf{y}) = [det(J_{T^{-1}}(\mathbf{y}))]^{-1} I_m(\mathbf{y})$. Assuming that the transformation function T is invertible, the determinant of Jacobian $J_{T^{-1}}(\mathbf{y})$ is the inverse of the determinant of Jacobian $J_T(\mathbf{x})$ and the modeled intensity of the moving image can be written as $\widehat{I}_m(\mathbf{y}) = det(J_T(\mathbf{x})) \cdot I_m(\mathbf{y})$.

Finally, the mass preserving intensity model can be naturally incorporated in the standard sum of square differences similarity function:

$$C(I_f, I_m \circ T) = \frac{1}{|\Omega_f|} \int_{\Omega_f} [I_f(\mathbf{x}) - det(J_T(\mathbf{x})) \cdot I_m(T(\mathbf{x}))]^2 d\mathbf{x}. \quad (3)$$

2.5. Optimization

In this paper we use a stochastic gradient descent method (Klein et al., 2007) to optimize the similarity function. The closed form expression for the gradient of the proposed mass preserving similarity function of Eq. (3) is,

$$\mathcal{D}_{\mathbf{a}} C = -\frac{2}{|\Omega_f|} \int_{\Omega_f} [I_f(\mathbf{x}) - det(J_T(\mathbf{x})) \cdot I_m(T(\mathbf{x}))] \cdot det(J_T(\mathbf{x})) \cdot \quad (4)$$
$$\cdot [\mathrm{vec}(J^{-T}(\mathbf{x}))^T \cdot \mathcal{D}_{\mathbf{a}} \mathrm{vec}(J(\mathbf{x})) \cdot I_m(T(\mathbf{x})) - \mathcal{D}_{\mathbf{y}} I_m(T(\mathbf{x})) \cdot \mathcal{D}_{\mathbf{a}} T(\mathbf{x})] \, d\mathbf{x},$$

where $\mathcal{D}_{\mathbf{a}}$ represents a gradient row vector operator with respect to the transformation parameters $\mathbf{a}$, $\mathcal{D}_{\mathbf{y}}$ represents a spatial gradient vector operator, and $vec(\cdot)$ is the vector constructed by concatenating all columns of a matrix. The derivation of Eq. (4) is given in the Appendix.

In case of SSD similarity function, only voxels with non-zero image gradient contribute to the gradient thus resulting in a higher uncertainty of registration in homogeneous regions (Hub et al., 2009). In contrast, for the proposed mass preserving similarity function of Eq. (4), voxels, where the image gradient $\mathcal{D}_{\mathbf{y}} I_m(\mathbf{y})$ is close to zero but intensities of the fixed and the deformed moving image are different also contribute to the gradient thus providing additional information in homogeneous regions.

3. Evaluation of image registration accuracy

The performance of image registration with the regular sum of squared differences similarity function (2) is compared to image registration with the proposed mass preserving similarity function (3) based on the vessel tree centerlines.

The vessels are segmented using the algorithm described in (Lo et al., 2010). First, the image is thresholded with fixed intensity $t_v = -380$ HU, followed by multi-scale local analysis of the Hessian matrix to remove non-tube like structures. Large vessels in the hylum area are discarded. Finally, centerlines are extracted from the segmented vessel tree using a 3D thinning algorithm (Wang and Basu, 2007). Fig. 1 shows an example of a segmented vessel tree and the centerlines extracted from it.

We measure image registration accuracy using the Euclidean distance between vessel tree centerlines. First, we extract vessels from both moving and fixed images. Next, the moving image vessel tree is deformed according to the final transformation coefficients. The vessel centerlines are extracted from the segmented vessel trees in fixed and deformed images. Then the Euclidean distance map is computed for the centerlines of the fixed image. Finally, the image registration error is computed as the Euclidean distance map values averaged over all centerline voxels in the deformed moving vessel tree.

Considering the large size of the data sets, as presented in this paper, the proposed evaluation approach offers an automatic alternative to the gold standard validation via manually annotated landmarks. Additionally, the registration accuracy on a subset of images is assessed using manually annotated landmarks.

4. Experiments and results

We performed three different experiments to study the proposed image registration method. The first experiment, described in Section 4.2, was designed to evaluate the assumption of mass preservation and to investigate the relationship between the volume of lungs and appearance of lung tissue. Section 4.3 illustrates the behaviour of the two registration methods, the proposed registration with mass preserving similarity function (MP) and the registration with sum of squared differences similarity function (SSD), on a synthetic example. Finally, the third experiment in Section 4.4 was designed to investigate how the difference in lung volume effects the two registration methods. Section 4.1 describes the parameter settings for the two registration methods used in all experiments.

4.1. Parameter settings

We applied three levels of B-Spline transformations, $N = 3$, with decreasing grid size. The first two levels were applied to the deformed, regridded moving image blurred Gaussian $\sigma_{1,2} = 1$ voxel and sampled by a factor of two in each direction. The third level was applied to the full resolution image without smoothing. The number of grid cells in each B-Spline level was $3 \times 3 \times 3$,$6 \times 6 \times 6$ and $12 \times 12 \times 12$ respectively. Optimal parameters were obtained by minimizing the cost function between the fixed and corresponding moving images.

After each level of transformation we deformed or regridded the original moving image and set the deformed image as a new moving image for the next level of transformation. The Jacobian of the transformation was computed using a first order difference scheme with the step equal to the image spacing.

Each of the four transformations in Eq. (1) was optimized separately using the stochastic gradient descent (Klein et al., 2007; Kushner and Yin, 2003). The number of voxel samples was chosen proportional to the number of parameters to optimize, and was set to 50,000 for the finest B-Spline transformation and to 10,000 for the intermediate B-Spline and Affine transformations. Maximum number of iterations was 1000 for all the transformations. The maximum step length along the normalized gradient direction was set to 0.5 mm.

Vessel trees were segmented using the algorithm as in (Lo et al., 2010). The intensity threshold was set to -400 HU for the scans in the experiments in Section 4.4.1, 4.4.2, and -600 for the scans in the experiments in Section 4.4.3, and the ratio of Hessian eigenvalues was set to $m_1 = 0.5$, $m_2 = 0.5$ for the experiments in Section 4.4.1 and 4.4.2 and $m_1 = 0.75$, $m_2 = 0.5$, for the experiments in Section 4.4.3. For more details on the parameters of the segmentation algorithm we refer reader to (Lo et al., 2010).

4.2. Experiment 1: relationship between mass, volume and density of lungs

We selected 797 subjects who were scanned annually during a 3 year period in a lung cancer screening program (Pedersen et al., 2009). None of the subjects suffered from Chronic Obstructive

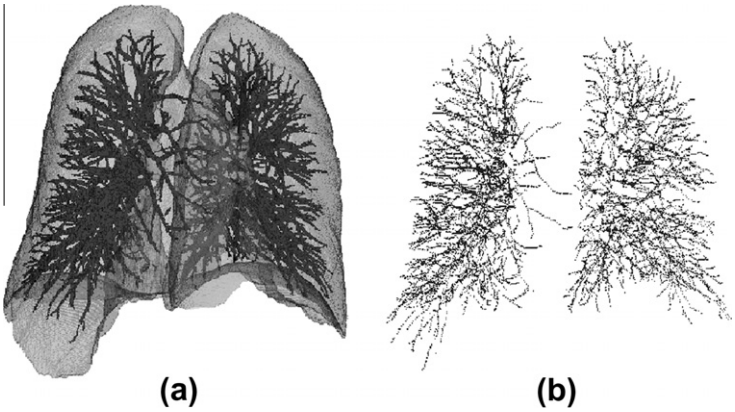

Fig. 1. Surface rendering of lung fields and vessels segmented (a) and corresponding vessel centerlines (b).

Pulmonary Disease (COPD) at any of the visits according to the GOLD guidelines (Rabe, 2007), so change in amount of lung tissue should be relatively small. We generated all possible pairs of scans of the same subject and randomly selected 1430 image pairs. Within the segmented lung mask, we computed total lung mass, total lung volume and average lung density for each pair of CT scans. Fig. 2a shows the scatter plot between relative change in total lung volume and change in total lung mass for the image pairs. Fig. 2b shows the scatter plot between relative change in total lung volume and change in average density. Spearman correlation between difference in mass and difference in volume was $r = 0.14$ ($p < 0.001$), and correlation between difference in average density and difference in volume was $r = -0.91$ ($p < 0.001$).

We investigated the relationship between total lung volume and the shape of histogram of a CT lung scan. The histogram of voxel intensities within the lungs mask was established with the uniform bins of 1 HU in the range of −1000–0 HU. We applied a simplified mass preserving model, where the lungs were assumed to expand or contract uniformly and the intensities were globally adjusted as

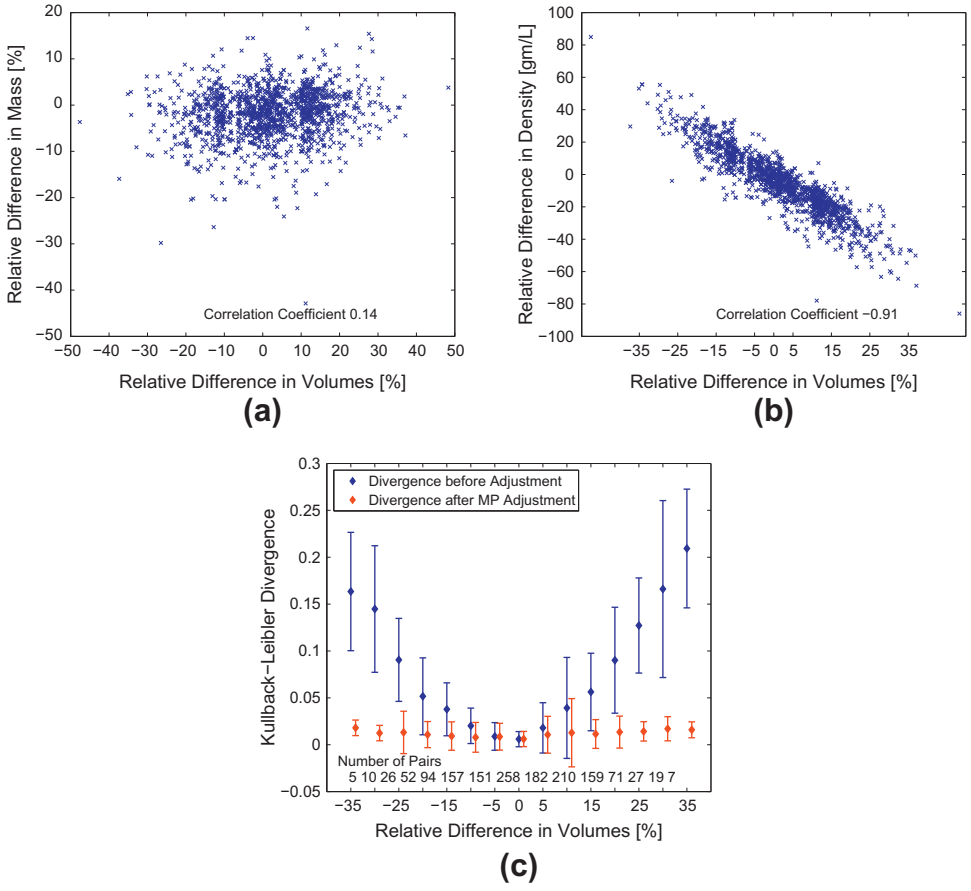

Fig. 2. Scatter plot visualizing the correlation between relative change in total lung volume and change in total lung mass (a) and average lung density (b). The most right plot displays the mean and the standard deviation of Kullback–Leibler divergence between histograms of two CT scans of the same subject (blue error bars). The divergence of the histograms of the same scans after intensities were adjusted for the volume difference is displayed in the same plot (red error bars). (For interpretation of the references to colour in this figure legend, the reader is referred to the web version of this article.)

$$\widehat{I}_1(\mathbf{x}) = \frac{V_1}{V_2}(1000 + I_1(\mathbf{x})) - 1000, \quad (5)$$

where the I_1 is the first image in a pair, the V_1 and V_2 is the total lung volume of the first and the second images in the pair. In order to account for empty bins, the histograms were smoothed with Gaussian $\sigma = 5$ HU. Finally, the histograms were normalized to represent probability distribution of the intensities. The difference between the probability distributions of intensity values of lung parenchyma before and after adjustment was assessed using the Kullback–Leibler divergence.

The 1430 pairs of CT scans were split into 15 groups with the relative volume difference varying from −37.5% to 37.5% of the mean lung volume of the two scans. For each group, the average and the standard deviation of the Kullback–Leibler divergence is reported in the Fig. 2c.

4.3. Experiment 2: synthetic data

The two image registration methods were evaluated on a synthetic image pair constructed to mimic lung tissue expansion under the mass preservation law. Both moving and fixed images represented uniform spheres placed in the center of the images with the background density 0 [g/L] (or intensity −1000 HU). The moving sphere S_1 had radius $r_1 = 16$ mm and density $\rho_1 = 200$ [g/L] (or intensity value $I_1 = -800$ HU) and the fixed sphere S_2 had radius $r_2 = 20$ mm and density $\rho_2 = 100$ [g/L] (or intensity value $I_2 = -900$ HU). The mass of the two spheres was approximately equal, 1.93 g and 1.89 g respectively.

The initial affine transformation was excluded from the image registration framework described in Section 2.3 and only the multi-level B-Spline transformations were used. Optimization parameters were identical for both image registration methods.

Fig. 3 shows the original fixed Fig. 3a and moving Fig. 3b spheres and the resulting difference between the registered and fixed images for the standard registration method Fig. 3c and the mass preserving method Fig. 3d.

4.4. Experiment 3: registration of lung CT scans

The third experiment was conducted on a large number of lung CT scans of varying quality, ranging from small to large differences in inspiration level.

- Group A: 44 image pairs of the same subject with the relative difference between total lung volumes for baseline and follow up images $\Delta TV < 2.5\%$, data obtained from a lung cancer screening study (Pedersen et al., 2009);
- Group B: 44 image pairs of the same subject with the relative difference between total lung volumes for baseline and follow up images $\Delta TV > 9\%$, data obtained from the lung cancer screening study (Pedersen et al., 2009);
- Group C: 16 image pairs of inspiratory and expiratory CT scans children with cystic fibrosis with the average relative difference between total lung volumes 48.3%, data obtained from a study (de Jong et al., 2004);
- Group D: 5 image pairs extracted at the end exhale and end inhale phases of the 4D-CT scans with the average relative difference between total lung volumes 11%, data obtained from the publicly available database (Castillo et al., 2009b).

For all four groups, we measured performance of the registration algorithms using the proposed evaluation technique described in Section 3. For the last group, 300 manually selected landmarks for each image pair were available. In this group we additionally compared the two registration methods with the landmark registration error.

4.4.1. Longitudinal study: groups A and B

Two groups of low dose CT image pairs were selected from the Danish Lung Cancer Trial Study (DLCST) database (Pedersen et al., 2009). Before the acquisition, subjects were instructed to hold their breath at maximum inspiration. Image pairs have a time interval between baseline and follow up of approximately one year. The in-plane resolution was 0.78×0.78 mm and the slice thickness was 1 mm. In the group A the average relative difference between the baseline and follow up lung volumes was 1.23 ± 0.77% and in the group B the average difference was 14.96 ± 5.84%.

Evaluation results for the two image registration methods are presented in the Table 1. For each patient, we computed the average distance between centerlines registered with the standard method and with the proposed mass preserving method. The overall improvement for each data set is presented in Fig. 4 with box plots showing median, lower and upper quartile, and skewness of the distribution within each group. The correlation between the relative difference in total lung volume and decrease in error of the mass preserving method in the two selected groups was $r = 0.44$ ($p < 0.001$).

The proposed method is computationally more demanding, due to a more complex gradient calculations of the cost function and non-optimized algorithm implementation. In the DLCST data, the proposed registration method on average required 1229 iterations or 77 min in total, whereas the standard registration required 840 iterations or 10 min in total.

4.4.2. Expiratory and inspiratory CT images: group C

The group C in our experiment consists of 16 children with cystic fibrosis (CF) monitored at Sophia Children's Hospital (de Jong et al., 2004). All children underwent biannual CT scanning during annual checkup during a clinically stable period. Each CT study consisted of a low-dose CT scan taken at maximum inspiration and an ultra low-dose scan taken at maximum expiration. Before the acquisition, subjects were instructed to exhale or inhale completely and to hold their breath. The in-plane resolution was on average 0.54×0.54 mm, the slice thickness is 2.5 mm with a slice

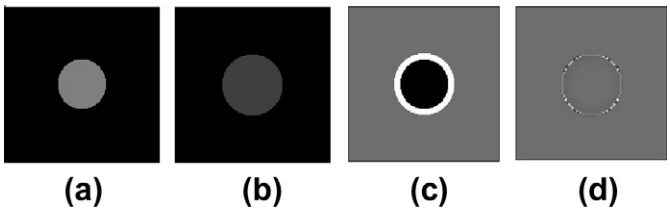

Fig. 3. The two image registration methods were applied to a synthetic example. The moving image Fig. 3b and fixed image Fig. 3a consist of spheres with equal mass, but different density. Results (difference image) of the standard image registration method Fig. 3c and the proposed mass preserving image registration method Fig. 3d.

Table 1
Average registration accuracy in each group, assessed using the vessel centerline distance, for the registration with the mass preserving (MP) and the sum of squared differences similarity function (SSD). Number in brackets indicates the number of subjects in the group.

Group	ΔTV (%)	ΔTV (L)	Vessel centerline distance (mm)		
			SSD	MP	*T*-test
A (44)	1.23 ± 0.77	0.07 ± 0.04	0.541 ± 0.258	0.539 ± 0.251	$p = 0.604$
B (44)	14.96 ± 5.84	0.83 ± 0.29	1.017 ± 0.634	0.987 ± 0.619	$p = 0.028$
C (16)	48.27 ± 19.69	1.53 ± 0.94	2.959 ± 1.370	2.535 ± 1.046	$p = 0.003$
D (5)	11.15 ± 2.86	0.37 ± 0.10	2.070 ± 0.519	2.038 ± 0.522	$p = 0.160$

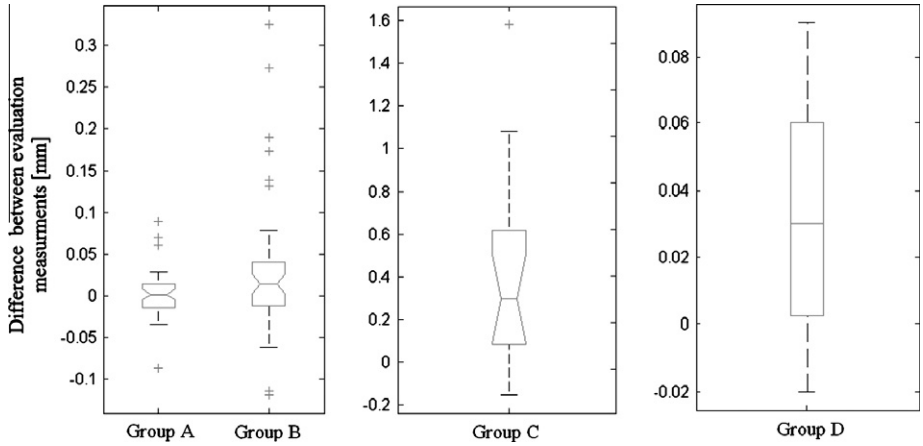

Fig. 4. Box plots showing the improvement in registration accuracy obtained by the mass preserving image registration method for each of the groups A–D. Each plot shows the median (central mark), lower and upper quartile (edges of the box), skewness of the distribution (notches) and outliers (crosses). From left to right: group A (44 subjects with average $\Delta TV = 1.23\%$), group B (44 subjects with average $\Delta TV = 14.96\%$), group C (16 subjects with $\Delta TV = 48.27\%$), group D (five subjects with average $\Delta TV = 11.14\%$).

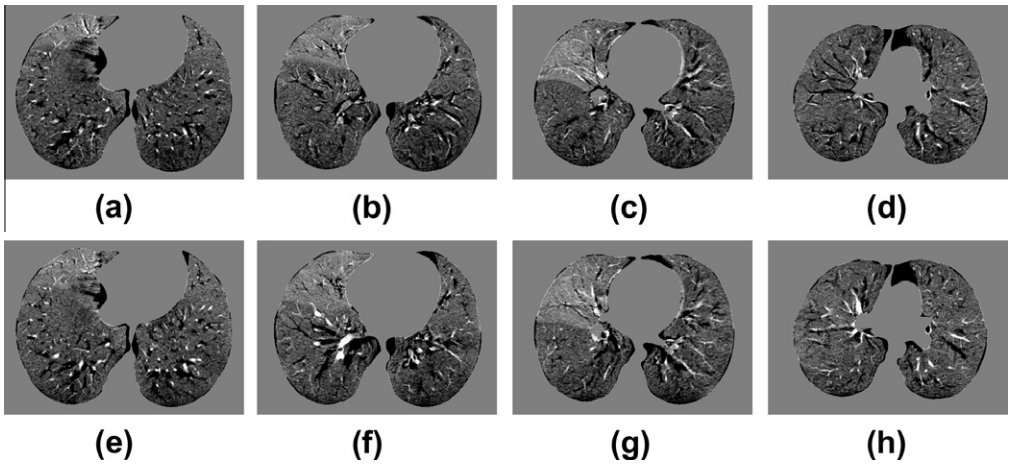

Fig. 5. An example illustrating the registration performance of mass preserving image registration Fig. 5a–d and standard registration Fig. 5e–h for a randomly selected subject from the group C. The difference images were constructed by first deforming the expiratory image and then subtracting it from the inspiratory image. Every 20th slice, selected in the range of 40–100 from the corresponding volumetric difference image is displayed from left to right.

Table 2
The two registration methods compared based on the proposed evaluation measure and the landmark registration error. Evaluation based on vessel-centerline distance and the validation based on the landmarks are reported before the registration (Initial), after the registration was applied with the mass preserving similarity function (MP), and with the sum of squared differences similarity function (SSD). The statistical comparison of the landmark registration errors is performed using Student's *t*-test and the *p*-value is reported in the last column.

		Vessel centerline distance (mm)			Landmark registration error (mm)			
N	ΔTV (%)	Initial	MP	SSD	Initial	MP	SSD	*p*-value
1	9.2	3.16 ± 2.17	1.38 ± 1.61	1.43 ± 1.61	3.99 ± 2.75	1.15 ± 0.55	1.18 ± 0.56	$p = 0.05$
2	8.9	4.64 ± 3.67	1.82 ± 2.35	1.80 ± 2.34	4.34 ± 3.90	1.26 ± 0.70	1.27 ± 0.68	$p = 0.53$
3	11.5	5.15 ± 3.80	2.16 ± 2.78	2.25 ± 2.79	6.93 ± 4.09	1.79 ± 1.08	1.88 ± 1.12	$p < 0.001$
4	15.9	4.86 ± 3.80	2.02 ± 2.26	2.05 ± 2.25	9.83 ± 4.86	2.01 ± 1.41	2.16 ± 1.54	$p < 0.001$
5	10.2	6.35 ± 6.42	2.81 ± 3.68	2.82 ± 3.65	7.51 ± 5.53	2.31 ± 1.89	2.29 ± 1.82	$p = 0.32$
All	11.14	4.83 ± 1.14	2.04 ± 0.52	2.07 ± 0.52	6.52 ± 4.83	1.70 ± 1.30	1.76 ± 1.32	$p < 0.001$

overlap of 1.3 mm. The difference in inspiration level between the two images was large on average, and many of the expiration scans show regions of trapped air, indicating local inhomogeneity of deformation. On average, the difference between inspiratory and expiratory volumes was 48.27 ± 19.69%. The inspiratory image was set as the fixed image.

Evaluation results are presented in the Table 1 and the overall improvement in the group C is presented in the box-plot Fig. 4. Correlation between the relative difference in total lung volume and improvement of the mass preserving method in the selected group was $r = 0.77$ ($p < 0.001$). Fig. 5 shows an example result of the two image registration techniques. The expiratory image was deformed according to the final transformation and subtracted from the inspiratory image. The two images show corresponding slices in the difference images for the mass preserving image registration technique Fig. 5a–d and for the standard registration Fig. 5e–h.

4.4.3. End exhale and end inhale CT images: group D

The last group D consists of a publicly available dataset of 5 pairs of images (Castillo et al., 2009b), where each pair consists of images extracted at the end exhale and the end inhale phases of 4D CT images. In-plane resolution of the images varied from 0.97×0.97 mm to 1.16×1.16 mm and slice thickness was 2.5 mm. The study (Castillo et al., 2009b) also provides 300 manually placed landmarks at the end exhale and end inhale phases of the 4D CT images. End exhale image was set as the fixed image.

We validated accuracy of the two image registration algorithms using two independent evaluation measures: the landmark registration error and the vessel centerline distance. The mean and the standard deviation of landmark registration error for each case is reported in the Table 2. The mean and the standard deviation of the vessel centerline distance for each case is also reported in the Table 2.

5. Discussion

5.1. Mass preservation in lung CT scans

The experiment in Section 4.2 showed a strong correlation between the change in average lung density and the change in total lung volume ($r = -0.91$, $p < 0.001$). This indicates a strong dependency of lung tissue appearance in CT scan on the level of inspiration. The correlation between the change in mass of the lungs and the change in total lung volume was weak but significant ($r = 0.14$, $p < 0.001$). This may be due to the incomplete vessel extraction, since inspiration leads to increase in perfusion and therefore to increase in partial volume effect near the vessels. It can also be due to increased perfusion outside the main vessels resulting in incomplete mass preservation.

A simplified intensity correction model based on the idea of mass preservation was investigated in the Section 4.2. Analysis of image histograms of healthy subjects from Fig. 2c confirmed the fact that the probability density function of image intensities significantly depends on the level of inspiration. Furthermore, the simplified global mass preserving intensity correction significantly reduced the divergence between the histograms as shown in Fig. 2c.

The results indicated that mass preservation is a plausible model of lung parenchyma, which models the change of lung tissue density caused by the change of total lung volume.

5.2. Mass preserving registration of lung CT images

The experiment in Section 4.3, conducted on synthetic data, illustrated the principle advantage of the proposed mass preserving registration, where mass preserving image registration leads to the expected alignment of two spheres that are equal in mass and different in volume. The SSD similarity function aligns equal intensities and in the presented synthetic data, intensities of the two spheres were different therefore the geometrically correct solution results in a larger value of the SSD similarity function than the initial positioning of the spheres. The mass preserving similarity function allows to align initially different intensities since the intensity is adjusted during the registration procedure thus resulting in the expected alignment of the spheres.

In cases, where image contrast differs between the images, the assumption of our model as well as the assumptions of the standard SSD similarity measure do not hold. However in the follow up studies, like the one considered in this paper, clinicians prefer to follow a standard acquisition protocol and reconstruction method and thus the difference in contrast should be negligible.

Although the constructed synthetic experiment is an exceptional example, the key advantage of mass preserving similarity function were clearly illustrated. Optimization for the sum of squared differences similarity function as well as the proposed mass preserving similarity function is mainly driven by high gradient structures in the moving image. In areas of high gradients both algorithms will converge to the correct solution, if they were initialized close to it. In absence of gradients the optimization of SSD similarity function will stop while the mass preserving similarity function will continue. For example, homogeneous areas in an expiration image with high intensities will tend to expand in case of mass preserving similarity function.

The advantage of mass preserving image registration is further confirmed in the third experiment. Especially in cases, where the difference in lung volume is large, which implies differences in regional ventilation and density. The group A of subjects in our experiments had negligible difference in lung tissue appearance between the two CT scans and the difference between the two methods was not significant ($p = 0.6$). In the group B, mass preserving image registration resulted in a relatively small, but statistically significant, improvement in registration accuracy compared to the standard image registration method (0.03 mm, $p = 0.03$). In group C, the most challenging group, a considerable and significant improvement was measured (0.43 mm, $p = 0.003$). The improvement in registration accuracy in groups A–C was strongly correlated with the relative difference in lung volume ($r = 0.78$, $p < 0.001$). In the last group D, the improvement of mass preserving registration assessed via manually selected landmarks was 0.06 mm, and was statistically significant ($p \leqslant 0.001$).

A mass preserving model predicts lung tissue appearance in CT scan during respiration based on a simple assumption: preservation of blood in lungs. The density of lung tissue is corrected locally, within the typical size of the B-Spline kernel, according to the change in regional ventilation as measured by the Jacobian of the deformation field. The limitation of this model is We previously applied this model for monitoring local emphysema progression in patients with COPD (Gorbunova et al., 2008). Recently, a similar study was done to monitor emphysema progression in patients with Alpha-1 antitrypsin deficiency (Staring et al., 2009), where a mass preserving intensity correction was applied after normal image registration to compensate for differences in inspiration level between scans. Results suggested more accurate estimates of the disease progression in both these studies.

5.3. Distance between vessel centerlines as a measure for registration accuracy

Manual extraction of landmarks is both time consuming and prone to inter-expert variability. In this work, instead of relying on manual landmarking we used an automated evaluation method based on vessel tree centerlines to assess the registration accuracy, resulting in a large number of approximately corresponding landmarks throughout the lungs. The drawback of the proposed evaluation is that vessels that are segmented in only one of the scans may lead to inflation of errors, whereas the absence of point correspondence may lead to underestimation of errors especially in regions, where vessel density is high. This could be improved for instance by determining corresponding vessel bifurcation points and parameterizing vessel segments in a consistent manner. However, the effects of over- and under-estimations can be expected to be similar for two different registration methods of the same scan pair provided that both registration methods are reasonably good, and the vessel tree distance is therefore well suited to compare registration accuracy of different methods on the same images.

Comparison with landmark registration error (TRE), available for the group D, showed that the vessel distance measure underestimated the errors before registration (the average vessel distance measure was 4.83 mm while the average TRE was 6.52 mm) and

resulted in overall overestimation of errors after the registration (2.40 mm versus 1.70 mm respectively).

5.4. Comparison to results in literature

In the conducted experiments, the proposed mass preserving image registration performed better than the registration with the sum of squared differences similarity function. The results of the registration with SSD similarity function was comparable with those reported in the literature. Most registration methods were evaluated on 4D-CT scans Castillo et al. (2009b), Yin et al. (2009b), Wu et al. (2008), Vik et al. (2008), Pevsner et al. (2006), Castillo et al. (2009a).

Wu et al. (2008) used manually extracted landmarks from four end exhale and end inhale image pairs from dynamic CT sequences to evaluate a B-Spline image registration algorithm and reported an average distance between landmarks of 2.78 mm. Pevsner et al. (2006) analyzed 6 pairs of end-exhale and end-inhale CT lung scans registered using a fluid registration method with 41 landmarks and reported a discrepancy between registered and observer-determined landmarks of 2.9 mm on average. Vik et al. (2008) evaluated a B-Spline image registration algorithm on a set of 10 pairs of end exhale and end inhale phases of 4D-CT lung scans with user-determined landmarks. The average distance between landmarks was 2.85 ± 3.06 mm. Castillo et al. (2009b) compared optical flow and landmark-based image registration algorithms on 5 pairs of end inhale and end exhale 4D-CT images as in our experiments. The average accuracy was 6.9 ± 0.1 mm for the optical flow image registration and 2.5 ± 0.02 mm for landmark-based registration. Another study by Castillo et al. (2009a) reported the average TRE of 1.59 mm obtained on the first 3 pairs of the end exhale and end inhale phases of 4D-CT scans. The target registration error of the proposed mass preserving registration method applied on the same 3 pairs end inhale and end exhale phases of 4D-CT scans was 1.40 mm on average.

In our experiments on group C, the pairs of maximum expiration and maximum inspiration CT lung scans, the average vessel distance after the mass preserving registration was relatively large, 2.53 mm. This group was the most challenging because of large difference in volume and expected large regional differences in ventilation due to pathology such as air-trapping and fibrotic tissue. In this group, the mass preserving registration showed clear improvement compared to the registration method with the SSD similarity function.

Registration of pairs of inspiratory lung CT scans generally produces more accurate results than can be obtained for expiration/inspiration scan pairs or end-exhale/end-inhale images from 4D-CT. Our experiments on longitudinal inspiratory CT lung scans showed comparable accuracy of mass preserving registration 0.76 mm to the results on similar studies reported in the literature (Betke et al., 2003; Murphy et al., 2008). Betke et al. (Betke et al., 2003) evaluated an image registration algorithm on 10 pairs of repeated inspiratory CT scans using RMS between corresponding surface points and measured error of 3.7 mm. Murphy et al. (Murphy et al., 2008) reported an average error of only 0.7 mm evaluated on a set of semi-automatically extracted landmarks. In this study, selection of landmarks was supported by a thin-plate spline landmark registration algorithm, potentially favoring smooth deformation fields.

6. Conclusion

In this paper we investigated the assumption of mass preservation during breathing cycle on a large number of CT scans, ranging from small to large difference in inspiration level. We incorporated the mass preserving model into a deformable image registration framework and evaluated it on synthetic data and pairs of lung CT scans acquired from the same subject. The results showed that the mass preserving model is a plausible model which describes the change in density in lung CT scans related to the change in lung volume. The mass preserving image registration performs significantly better than the image registration method without mass preservation assumption in image pairs with a considerable difference in inspiration level. Especially in regions without strong image gradients, the mass preserving assumption helps to obtain physically plausible deformations.

Acknowledgment

This work was financially supported by the Danish Council for Strategic Research under the Program Commission for Nanoscience and Technology, Biotechnology and IT (NABIIT), the Netherlands Organization for Scientific Research (NWO), and AstraZeneca, Lund, Sweden.

We would like to thank Saher B. Shaker of the Department of Cardiology and Respiratory Medicine, Hvidovre University Hospital, Copenhagen, Denmark, and Haseem Ashraf of the Department of Respiratory Medicine, Gentofte University Hospital, Denmark, for fruitful discussions and insight into the physiological behavior of the lungs during respiratory cycle. We also thank Stefan Klein of the Biomedical Imaging Group Rotterdam, Erasmus Medical Center, Rotterdam, the Netherlands, for useful suggestions on the implementation.

Appendix A. Gradient of the mass preserving similarity function

In this section we derive the analytical expression for the gradient of the proposed mass preserving similarity function as given in Eq. (4). Consider the similarity function (as in Eq. (3)):

$$C(I_f, I_m \circ T) = \frac{1}{|\Omega_f|}\int_{\Omega_f} [I_f(\mathbf{x}) - det(J_T(\mathbf{x}))\cdot I_m(T(\mathbf{x}))]^2 d\mathbf{x}. \tag{A.1}$$

The transformation function $T(\mathbf{x})$ depends on the set of parameters $\mathbf{a}$, $T(\mathbf{a}, \mathbf{x})$. For simplicity, we shorten the notation of the Jacobian determinant $|J| = det(J_T(\mathbf{x}))$, the fixed image value in a point $\mathbf{x}$ as $I_f = I_f(\mathbf{x})$, the transformed point $\mathbf{y} = T(\mathbf{x}, \mathbf{a})$, the moving image value in the transformation point $I_m = I_m(\mathbf{y})$ and label the observed difference in intensities at a point $\mathbf{x}$ with respect to the transformation parameters $\mathbf{a}$ as a function $G(\mathbf{a}, \mathbf{x})$:

$$C(I_f, I_m \circ T(\mathbf{a})) = \int_{\Omega_f} G(\mathbf{a},\mathbf{x})^2 \, d\mathbf{x},$$
$$G(\mathbf{a},\mathbf{x}) = I_f(\mathbf{x}) - det(J_T(\mathbf{x}))\cdot I_m(\mathbf{y}(\mathbf{a},\mathbf{x})) = I_f - |J| I_m.$$

Using differential algebra we write the full differential of the similarity function

$$dC(\mathbf{a}) = \int_{\Omega_f} 2GdG \, d\mathbf{x},$$
$$dG(\mathbf{a},\mathbf{x}) = \mathcal{D}_{\mathbf{x}} I_f d\mathbf{x} - |J|\mathrm{tr}(J^{-1}dJ) I_m - |J|\mathcal{D}_{\mathbf{y}} I_m d\mathbf{y}$$
$$= \mathcal{D}_{\mathbf{x}} I_f \, d\mathbf{x} - |J|\left(\underbrace{\mathrm{tr}(J^{-1}dJ)}_{(1)} I_m + \mathcal{D}_{\mathbf{y}} I_m d\mathbf{y}\right). \tag{A.2}$$

Using the definition of the vec operator, we can simplify the term (1):

$$\mathrm{tr}\,(J^{-1}dJ) = \mathrm{vec}(J^{-T})^T \mathrm{vec}(dJ). \tag{A.3}$$

Further the term vec (dJ) can be expanded,

$$\mathrm{vec}(dJ) = d(\mathrm{vec}(J)) = \mathcal{D}_{\mathbf{a}}\mathrm{vec}(J)\, d\mathbf{a} + \mathcal{D}_{\mathbf{x}}\mathrm{vec}(J)\, d\mathbf{x}, \tag{A.4}$$

and by substituting Eq. (A.4) into Eq. (A.3) we get

$$\mathrm{tr}\ (J^{-1}dJ) = \mathrm{vec}(J^{-T})^T \cdot \mathcal{D}_{\mathbf{a}}\mathrm{vec}(J)\ d\mathbf{a} + \mathrm{vec}(J^{-T})^T \cdot \mathcal{D}_{\mathbf{x}}\mathrm{vec}(J)\ d\mathbf{x}, \tag{A.5}$$

where $\mathcal{D}_{\mathbf{a}}$ is the gradient in the direction of the transformation parameters $\mathbf{a}$ and $\mathcal{D}_{\mathbf{x}}$ is a spatial gradient. The differential $d\mathbf{y}$ is defined as

$$d\mathbf{y} = \mathcal{D}_{\mathbf{a}}\mathbf{y}\ d\mathbf{a} + \mathcal{D}_{\mathbf{x}}\mathbf{y}\ d\mathbf{x} = \mathcal{D}_{\mathbf{a}}\mathbf{y}\ d\mathbf{a} + J\ d\mathbf{x}. \tag{A.6}$$

By substituting Eqs. (A.5) and (A.6) into Eq. (A.2) we get the full differential of $C(I_f, I_m \circ T)$:

$$dG(\mathbf{a},\mathbf{x}) = \mathcal{D}_{\mathbf{x}}I_f\ d\mathbf{x} - |J| \cdot \mathcal{D}_y I_m \cdot J\ d\mathbf{x} - |J| \cdot I_m \cdot \mathrm{vec}(J^{-T})^T \cdot \mathcal{D}_x\mathrm{vec}(J)\ d\mathbf{x} - |J| \cdot \mathrm{vec}(J^{-T})^T \cdot \mathcal{D}_{\mathbf{a}}\mathrm{vec}(J)\ d\mathbf{a} - |J| \cdot \mathcal{D}_y I_m \cdot \mathcal{D}_{\mathbf{a}}\mathbf{y}\ d\mathbf{a}.$$

Finally, since $\mathbf{x}$ is fixed, we find that the partial derivative of $C(I_f, I_m \circ T)$, w.r.t. the transformation parameters $\mathbf{a}$ is

$$\mathcal{D}_{\mathbf{a}}C = -\frac{1}{\Omega_f}\int_{\Omega_f} 2(I_f - |J| \cdot I_m) \cdot |J| \cdot (\mathrm{vec}(J^{-T})^T \cdot \mathcal{D}_{\mathbf{a}}\mathrm{vec}(J) \cdot I_m - \mathcal{D}_{\mathbf{y}}I_m \cdot \mathcal{D}_{\mathbf{a}}\mathbf{y})\ d\mathbf{x},$$

where $\mathcal{D}_{\mathbf{y}}I_m = (\partial_{y_1}I_m; \partial_{y_2}I_m; \partial_{y_3}I_m)$ is the spatial row-vector gradient and $\mathcal{D}_{\mathbf{a}}$ is the row-vector gradients the transformation $T(\mathbf{x}) = \mathbf{y} = (y_1; y_2; y_3)$ in the direction of the transformation parameters $\mathbf{a}$,

$$\mathcal{D}_{\mathbf{a}}\mathbf{y} = \begin{pmatrix} \partial_{a_1}y_1 & \dots & \partial_{a_n}y_1 \\ \partial_{a_1}y_2 & \dots & \partial_{a_n}y_2 \\ \partial_{a_1}y_3 & \dots & \partial_{a_n}y_3 \end{pmatrix}. \tag{A.7}$$

References

Betke, M., Hong, H., Thomas, D., Prince, C., Ko, J.P., 2003. Landmark detection in the chest and registration of lung surfaces with an application to nodule registration. Medical Image Analysis 7, 265–281.

Boldea, V., Sharp, G.C., Jiang, S.B., Sarrut, D., 2008. 4D-CT lung motion estimation with deformable registration: quantification of motion nonlinearity and hysteresis. Medical Physics 35, 1008–1018.

Castillo, E., Castillo, R., Zhang, Y., Guerrero, T., 2009a. Compressible image registration for thoracic computed tomography images. Journal of Medical and Biological Engineering 29, 236–247.

Castillo, R., Castillo, E., Guerra, R., Johnson, V.E., McPhail, T., Garg, A.K., Guerrero, T., 2009b. A framework for evaluation of deformable image registration spatial accuracy using large landmark point sets. Physics in Medicine and Biology 54, 1849–1870.

Christensen, G.E., Song, J.H., Lu, W., Naqa, I.E., Low, D.A., 2007. Tracking lung tissue motion and expansion/compression with inverse consistent image registration and spirometry. Medical Physics 34 (6), 2155–2164.

Ding, K., Bayouth, J., Buatti, J., Christensen, G., Reinhardt, J., 2010. 4D CT-based measurement of changes in pulmonary function following a course of radiation therapy. Medical Physics 37, 1261–1272.

Gorbunova, V., Lo, P., Ashraf, H., Dirksen, A., Nielsen, M., de Bruijne, M., 2008. Weight preserving image registration for monitoring disease progression in lung CT. In: Metaxas, D., Axel, L., Székely, G., Fichtinger, G. (Eds.), Proc. Medical Image Computing and Computer Assisted Intervention (MICCAI), pp. 863–870.

Gorbunova, V., Lo, P., Loeve, M., Tiddens, H., Sporring, J., Nielsen, M., de Bruijne, M., 2009. Mass preserving registration for lung CT. In: Pluim, J., Dawant, B. (Eds.), SPIE (Medical Imaging).

Guerrero, T., Sanders, K., Castillo, E., Zhang, Y., Bidaut, L., Pan, T., Komaki, R., 2006. Dynamic ventilation imaging from four-dimensional computed tomography. Physics in Medicine and Biology 51, 777–791.

Guerrero, T., Zhang, G., Segars, W., Huang, T.C., Bilton, S., Ibbott, G., Dong, L., Forster, K., Lin, K.P., 2005. Elastic image mapping for 4-D dose estimation in thoracic radiotherapy. Radiation Protection Dosimetry 115, 497–502.

Hill, D.L., Batchelor, P.G., Holden, M., Hawkes, D.J., 2001. Medical image registration. Physics in Medicine and Biology 46, R1–45.

Hong, H., Lee, J., Yim, Y., 2008. Automatic lung nodule matching on sequential CT images. Computers in Biology and Medicine 38, 623–634.

Hub, M., Kessler, M.L., Karger, C.P., 2009. A stochastic approach to estimate the uncertainty involved in b-spline image registration. IEEE Transactions on Medical Imaging 28, 1708–1716.

de Jong, P., Nakano, Y., Lequin, M., Woods, R., Pare, R., Tiddens, H., 2004. Progressive damage on high-resolution computed tomography despite stable lung function in CF. European Respiratory Journal 23, 93–97.

Kabus, S., von Berg, J., Yamamoto, T., Opfer, R., Keall, P.J., 2008. Lung ventilation estimation based on 4D-CT imaging. In: Brown, M., de Bruijne, M., van Ginneken, B., Kiraly, A., Kuhnigk, J., Lorenz, C., Mori, K., Reinhardt, J. (Eds.), First International Workshop on Pulmonary Image Analysis, pp. 73–83.

Klein, S., Staring, M., Pluim, J.P.W., 2007. Evaluation of optimization methods for nonrigid medical image registration using mutual information and B-splines. IEEE Transactions on Image Processing 16, 2879–2890.

Kushner, H., Yin, G., 2003. Stochastic Approximation and Recursive Algorithms and Applications. Springer-Verlag, New York.

Li, P., Malsch, U., Bendl, R., 2008. Combination of intensity-based image registration with 3D simulation in radiation therapy. Physics in Medicine and Biology 53, 4621–4637.

Lo, P., Sporring, J., Ashraf, H., Pedersen, J.J., de Bruijne, M., 2010. Vessel-guided airway tree segmentation: a voxel classification approach. Medical Image Analysis 14, 527–538.

Mattes, D., Haynor, D., Vesselle, H., Lewellen, T., Eubank, W., 2003. PET-CT image registration in the chest using free-form deformations. IEEE Transactions on Medical Imaging 22, 120–128.

Murphy, K., van Ginneken, B., Pluim, J., Klein, S., Staring, M., 2008. Semi-automatic reference standard construction for quantitative evaluation of lung CT registration. In: Metaxas, D., Axel, L., Székely, G., Fichtinger, G. (Eds.), Proc. Medical Image Computing and Computer Assisted Intervention (MICCAI), pp. 1006–1013.

Murphy, K., van Ginneken, B., van Rixkoort, E.M., de Hoop, B.J., Prokop, M., Lo, P., de Bruijne, M., Pluim, J.P.W., 2009. Obstructive pulmonary function: Patient classification using 3D registration of inspiration and expiration CT images. In: Second International Workshop on Pulmonary Image Analysis.

Pedersen, J., Ashraf, H., Dirksen, A., Bach, K., Hansen, H., Toennesen, P., Thorsen, H., Brodersen, J., Skov, B., Døssing, M., Mortensen, J., Richter, K., Clementsen, P., Seersholm, N., 2009. The Danish randomized lung cancer CT screening trial – overall design and results of the prevalence round. Journal of Thoracic Oncology 4, 608–614.

Pevsner, A., Davis, B., Joshi, S., Hertanto, A., Mechalakos, J., Yorke, E., Rosenzweig, K., Nehmeh, S., Erdi, Y., Humm, J., Larson, S., Ling, C., Mageras, G., 2006. Evaluation of an automated deformable image matching method for quantifying lung motion in respiration-correlated CT images. Medical Physics 33, 369–376.

Rabe, K. et al., 2007. Global strategy for the diagnosis, management, and prevention of chronic obstructive pulmonary disease gold executive summary. American Journal of Respiratory and Critical Care Medicine 176, 532–555.

Reinhardt, J.M., Ding, K., Cao, K., Christensen, G.E., Hoffman, E.A., Bodas, S.V., 2008. Registration-based estimates of local lung tissue expansion compared to xenon CT measures of specific ventilation. Medical Image Analysis 12, 752–763.

Rueckert, D., Aljabar, P., Heckemann, R.A., Hajnal, J.V., Hammers, A., 2006. Diffeomorphic registration using b-splines. In: Larsen, R., Nielsen, M., Sporring, J. (Eds.), Proc. Medical Image Computing and Computer Assisted Intervention (MICCAI), pp. 702–709.

Rueckert, D., Sonoda, L.I., Hayes, C., Hill, D.L.G., Leach, M.O., Hawkes, D.J., 1999. Nonrigid registration using free-form deformations: application to breast MR images. IEEE Transactions on Medical Imaging 18, 712–722.

Sarrut, D., Boldea, V., Miguet, S., Ginestet, C., 2006. Simulation of 4D-CT Images from deformable registration between inhale and exhale breath-hold CT scans. Medical Physics 33, 605–617.

Shaker, S.B., Dirksen, A., Laursen, L.C., Skovgaard, L.T., Holstein-Rathlou, N.H., 2004. Volume adjustment of lung density by computed tomography scans in patients with emphysema. Acta Radiologica 4.

Simon, B., 2000. Non-invasive imaging of regional lung function using X-ray computed tomography. Journal of Clinical Monitoring and Computing 16, 433–442.

Sluimer, I., Prokop, M., van Ginneken, B., 2005. Towards automated segmentation of the pathological lung in CT. IEEE Transactions on Medical Imaging 24, 1025–1038.

Sluimer, I., Schilham, A., Prokop, M., van Ginneken, B., 2006. Computer analysis of computed tomography scans of the lung: a survey. IEEE Transactions on Medical Imaging 25, 385–405.

Staring, M., Bakker, M., Shamonin, D., Stolk, J., Reiber, J., Stoel, B., 2009. Towards local estimation of emphysema progression using image registration. In: Pluim, J., Dawant, B. (Eds.), SPIE (Medical Imaging).

Staring, M., Klein, S., Pluim, J.P., 2007. A rigidity penalty term for nonrigid registration. Medical Physics 34, 4098–4108.

Ue, H., Haneishi, H., Iwanaga, H., Suga, K., 2007. Respiratory lung motion analysis using a nonlinear motion correction technique for respiratory-gated lung perfusion SPECT images. Annals of Nuclear Medicine 21, 175–183.

Vik, T., Kabus, S., von Berg, J., Ens, K., Dries, S., Klinder, T., Lorenz, C., 2008. Validation and comparison of registration methods for free-breathing 4D lung-CT. In: Reinhardt, J.M., Pluim, J.P.W. (Eds.), SPIE (Medical Imaging).

Wang, T., Basu, A., 2007. A note on a fully parallel 3D thinning algorithm and its applications. Pattern Recognition Letters 28 (4), 501–506.

Wu, Z., Rietzel, E., Boldea, V., Sarrut, D., Sharp, G.C., 2008. Evaluation of deformable registration of patient lung 4DCT with subanatomical region segmentations. Medical Physics 35, 775–781.

Yin, Y., Hoffman, E., Lin, C.L., 2009a. Local tissue-weight-based nonrigid registration of lung images with application to regional ventilation. In: Pluim, J., Dawant, B. (Eds.), SPIE (Medical Imaging).

Yin, Y., Hoffman, E.A., Lin, C.L., 2009b. Mass preserving nonrigid registration of CT lung images using cubic B-spline. Medical Physics 36 (9), 4213–4222.

Zhang, L., Hoffman, E.A., Reinhardt, J.M., 2006. Atlas-driven lung lobe segmentation in volumetric X-ray CT images. IEEE Transactions on Medical Imaging 25, 1–16.

Zheng, Y., Steiner, K., Bauer, T., Yu, J., Shen, D., Kambhamettu, C., 2007. Lung nodule growth analysis from 3D CT data with a coupled segmentation and registration framework. In: MMBIA Workshop at IEEE 11th International Conference on Computer Vision, pp. 1–8.

Zhu, L., Yang, Y., Haker, S., Tannenbaum, A., 2007. An image morphing technique based on optimal mass preserving mapping. IEEE Transactions on Image Processing 16, 1481–1495.